N76-28183

A SUBVORTEX TECHNIQUE FOR THE CLOSE APPROACH TO A DISCRETIZED VORTEX SHEET+

Brian Maskew
Analytical Methods, Inc.

SUMMARY

The close-approach problem associated with vortex-lattice methods was examined numerically with the objective of calculating velocities at arbitrary points, not just at midpoints, between the vortices. The objective was achieved using a subvortex technique in which a vortex splits into an increasing number of subvortices as it is approached. The technique, incorporated in a two-dimensional potential flow method using "submerged" vortices and sources, was evaluated for a cambered Joukowski airfoil. The method could be extended to three dimensions, and should improve non-linear methods, which calculate interference effects between multiple wings and vortex wakes, and which include procedures for force-free wakes.

INTRODUCTION

A fundamental problem associated with vortex-lattice methods (e.g., ref. 1) is that appreciable errors can occur in velocities calculated close to the discretized vortex sheets because of the singular nature of the induced velocity expression. This problem has been circumvented in the past by calculating "near-field" velocities only at special points, e.g., midway between the vortices, and by employing interpolation for intermediate positions. For calculations involving multiple vortex sheets, (e.g., refs. 2 and 3), the near-field problem often requires that adjacent lattices be made to correspond across the gap between the sheets. However, such a solution is not practical in vortex-lattice methods which incorporate iterative procedures for force-free wakes, (refs. 3 through 11). Although these methods have proved very versatile in general, close-approach situations involving multiple discretized vortex sheets require careful treatment, and, ideally, the near-field problem should be removed.

The objective of this investigation was to develop a near-field modification for the discrete vortices which would allow velocities to be calculated anywhere in the flow field, not just at the special points. Such a capability would particularly benefit the analysis of high-lift configurations and the calculation of other close interference effects between wings and vortex sheets

+This work was performed while the author was a National Research Council Associate at the NASA Ames Research Center.

(or vortices) such as occur in configurations with leading-edge or tip-edge vortices.

Although the present paper deals with the near-field problems in two-dimensional flow, the extension to three dimensions (particularly for methods having a force-free wake) is a major consideration throughout. The development of the technique described herein is presented in more detail in references 12 and 13.

EXTENT OF THE NEAR-FIELD REGION

To evaluate the extent of the near-field region, the velocity distribution was examined for a flat, two-dimensional vortex sheet with a parabolic vorticity distribution (ref. 12). This distribution was discretized using forty vortices with equal spacing, Δ. Velocity distributions were calculated over a region between two midpoints near the quarter position on the segment (fig. 1(a)) and compared with the analytic values. Error contours are shown in figure 1(b). The discretization gives negligible errors for both components of velocity in the region beyond 1Δ from the sheet. In effect, the "holes" in the representation are not sensed until we enter the 1Δ region. Inside the 1Δ region the errors increase rapidly except along special lines of approach to the sheet. For the normal velocity component, the zero-error lines follow approximately the normals to the sheet at the points midway between the vortices and also at the vortices. (Deviations from the normal lines occur because of the gradient in vorticity across the region.) Both sets of positions on the surface are used in the non-linear vortex-lattice method, (e.g., ref. 3), i.e., the midpoints are used as control points, as in the standard vortex-lattice theory, and the vortex points are used when applying the Kutta-Joukowski law for local forces and also when performing the trailing-vortex roll-up calculations. The zero-error lines for the tangential velocity component are less well known; these lines enter the near-field region above the quarter and three-quarter positions between the vortices, and approach the vortex locations along approximately elliptical paths. All the zero-error paths are situated on extreme "precipices" in the error contour map; small deviations from the paths result in large errors and lead to the near-field problems.

NEAR-FIELD MODELS

The previous section indicated that errors arising from the discretization of a vortex sheet become appreciable only within the 1Δ region. Clearly, if we wished to calculate velocities very close to the discretized vortex sheet, we could simply decrease the size of Δ by increasing the number of vortices; however, for three-dimensional problems the computing time could then become prohibitive. An alternative solution is to apply a near-field treatment to the vortices. This treatment would be applied only to those vortices that are within a specified near-field radius (e.g., 1Δ) from the point where the velocity is being calculated. A number of near-field models were considered.

A core model offers the simplest near-field treatment which removes the singular behavior of the velocity field. In such a model the velocity induced by the vortex is factored locally so as to remain bounded at the vortex center. The Rankine vortex and Lamb's viscous vortex are well known examples, but there are other possible forms. Core models have been used in the past to smooth the motions of vortices used in two-dimensional roll-up calculations (e.g. refs. 14 and 15). Several core models were tested using the discretized parabolic vorticity sheet, but none were found satisfactory for both components of velocity. For example, they fail to restore the tangential component of velocity near the vortex sheet. This can be seen in figure 2, which shows the error contours for a Rankine vortex model with a core diameter of Δ. Although the tangential velocity errors appear slightly worse than for the unmodified vortex (compare figs. 1(b) and 2), the normal component errors are improved, on the whole, within the core. But the error levels are still significant, and the zero-error lines no longer approach the vortex points. Other near-field models were, therefore, considered in which the vortex itself is modified, its strength being effectively distributed along a line representing the local position of the vortex sheet. This investigation led to the subvortex technique.

SUBVORTEX TECHNIQUE

A technique was developed in which the strength of a near-field vortex is distributed by splitting it into a number of small vortices, i.e., subvortices. These are distributed evenly along the vortex sheet joining the vortex to its two immediate neighbors. The joining sheet is not necessarily a straight line; the subvortices can be placed on an interpolated curve passing through the basic vortices, and this allows a close representation of curved vortex sheets. Half intervals separate the basic vortices from the nearest subvortices (fig. 3(a)), and so the basic vortex positions become midpoints in the subvortex system. This feature improves the accuracy of the calculated velocity at the basic vortices (see "error contours").

The subvortices must have a combined strength equal to that of the associated basic vortex. In the technique as used here, their strengths vary linearly with distance from the basic vortex position. When several neighboring basic vortices are treated in this way, the local effect approaches that of a piecewise linear vorticity distribution. Clearly, higher order distributions could be used, but would involve more than one basic vortex interval on each side.

The number of subvortices used is such that the point where the velocity is being calculated cannot "see the holes" in the discretized vortex sheet, i.e., the point is kept just outside the new local 1Δ region of the subvortex system. Figure 3(b) shows how this works using the following expression for the number of subvortices on one side of the basic vortex:

$$\text{NSV} = \text{integer-part-of } (1 + \Delta/H) \qquad (1)$$

where H is the normal distance of the point from the segment. Use of this expression keeps the number of subvortices to a minimum and helps to keep compu-

ting costs down. When applied to the vortex-lattice methods, the midpoints between the vortices (i.e., the control points) should remain midpoints in the subvortex system; NSV must then be even, i.e., as shown dotted in fig. 3(b).

A maximum limit, NSV_{MAX}, is placed on the number of subvortices to avoid a runaway condition when the height H approaches zero. This limit controls the closest approach that can be made to the vortex sheet before the new local 1Δ region of the subvortices is entered. It can therefore be used to control the "accuracy" of the calculation in a trade-off with computing time, i.e., by increasing the limit the error region would decrease in size, but the computing time would increase, and vice-versa. To minimize calculation errors inside the 1Δ region of the subvortex system, each subvortex has been modified with a Rankine vortex core of diameter slightly less than the subvortex spacing. This smears out the tangential velocity discontinuity associated with the vortex sheet, but only over the new, diminished error-region. When representing free vortex sheets, this smeared region could be related to the thickness of the viscous wake in real flow.

Although the velocity errors become significant only within the 1Δ region, the near-field radius, within which the subvortex technique is applied, had to be increased to 5Δ to obtain the required accuracy ($\pm$ 0.5% error). The reason for this extension is that the induced velocity from the "distributed" model does not match that from the basic vortex until some distance away (ref. 12).

Error Contours

The technique was tested on the discretized parabolic vorticity distribution considered earlier. The error contours (fig. 4) are reduced to a very small region adjacent to the vortex sheet where the approach is closer than the subvortex spacing. The extent of this error region depends on the maximum limit placed on the number of subvortices. In these calculations NSV_{MAX} was 10.

The normal component of velocity calculated at the vortex locations has always been slightly less accurate than that calculated at points midway between the vortices. (The vortex points are effectively midpoints in a coarser discretization.) For the present discretized parabolic vorticity distribution, the error at the vortices in the region considered (see fig. 1(a)) is 2.8% compared with 0.03% at the midpoints. With the subvortex technique applied, the error at the vortices decreases to 0.2%; this reduction is helped by the fact that the basic vortex locations become midpoints in the subvortex system.

SUBMERGED SINGULARITIES

The subvortex technique was incorporated in a two-dimensional potential flow method (ref. 13) aimed at calculating pressures at arbitrary points on airfoil surfaces. For this purpose, the error region associated with the subvortex system was enclosed in the contour by "submerging" the vortices a small

distance below the surface (fig. 5). The basic vortices (before submerging) were positioned on the airfoil surface using equal angle increments in a cosine equation applied to distance along the contour. In this spacing system, half angles separate the initial vortex positions from the control points where the boundary condition of tangential flow is specified. This is an adaptation of Lan's work (ref. 16); it keeps the singularity strength distribution more uniform when passing through "difficult" regions such as leading and trailing edges and flap hinge lines. With this point distribution, the first control point is located at the trailing edge, and so the Kutta condition is applied by specifying the flow direction there, e.g., the direction along the mean line.

From their initial surface positions, the basic vortices are submerged along the local normals to the surface by a fraction of Δ, i.e., SDFΔ. The submerged depth factor, SDF, is constant over the whole contour except in the trailing-edge region where it automatically decreases along the single sheet (fig. 5). The control points remain on the airfoil contour except in the region very close to the trailing edge; here, corresponding upper and lower control points are combined and moved to the mean line. Hence, the model adjacent to the trailing edge resembles a camber line model. Because of this modelling, there are more control points than unknown singularities, and so the equations are solved in a least-squares sense.

The subvortices are placed on straight segments joining the basic vortices (see fig. 6). They are positioned in accordance with equal angle increments in the same system as the basic vortices (ref. 13).

For the three-dimensional case, quadrilateral vortices have been found convenient for modelling arbitrary geometry configurations (refs. 2,3 and 11). The present study, therefore, is based on the two-dimensional form of that model, viz., opposing vortex pairs, (fig. 6), which are equivalent to a piecewise uniform normal doublet distribution. Such a model, forming a closed surface, requires one doublet panel strength to be specified, otherwise the system is indeterminate. Accordingly, the upper panel adjacent to the crossover (fig. 6) is specified to have zero strength. The boundary condition equation associated with the control point above the specified panel is still included in the system of equations. The resultant vortex strengths are:

$$\Gamma_k = D_k - D_{k+1}; \; k = 1, 2, \ldots, N \qquad (2)$$

where D_k are the doublet panel strengths, i.e., the strengths of the opposing vortex pairs. (Note that D_{N+1} has been assumed zero.)

Preliminary calculations using vortices alone (ref. 13) showed problems near the leading edge and near the crossover of the interior vortex "sheets". These problems were attributed to ill-conditioning of the boundary equations, particularly near the crossover, because the vortices were trying to provide thickness effects (as well as lifting effects) from a small base. Source singularities, which are more suitable for providing thickness effects, were therefore included in the model. The sources, coincident with the vortices and

receiving the same "subvortex" treatment, have a simple strength distribution which provides the basic thickness form symmetrically about the mean line (ref. 13). The sources particularly benefit the pressure calculations in the leading- and trailing-edge regions.

RESULTS AND DISCUSSION

Figure 7 shows the pressure distribution calculated at 120 surface points that are not related to the vortex/control point locations. The airfoil is a cambered Joukowski represented by 46 vortex/sources with a submerged depth of 0.1 and a near-field radius of 5 . Trapezoidal-rule integration of the pressure distribut on yields the following lift, drag and moment coefficients: C_L = 1.7040 (0.4% error); C_D = -0.0069 (an error of 0.4% of C_L); and C_M = -0.5377 (0.26% error). The calculated pressure values show good agreement with the exact distribution, but they show a minor tendency to oscillate near the leading edge. The oscillations can be reduced (ref. 13) by increasing the density of the subvortex system, but the computing time increases (53% increase in time for a factor of 2 on the number of subvortices). Use of a higher order interpolation scheme for positioning the subvortices also reduces the oscillatory tendency (ref. 13). The oscillations can be eliminated by using a large number of basic singularities (e.g., 90). It is significant that the small oscillation disappears when there is no suction peak, e.g., figure 8 shows the pressure distribution for the same airfoil at zero incidence, the C_D error in this case being 0.0002 or 0.4% of C_L. (This case had the higher-order geometry routine for positioning the subvortices.) This implies that a higher-order strength variation for the subvortices might be useful when using only a small number of basic singularities; this would ensure that peaks in the pressure distribution are adequately represented. The higher-order routines would only be applied locally in the problem areas.

Figure 9 shows the pressures calculated at the same 120 arbitrary points as before, but with only 19 basic singularities; using so few vortex unknowns would clearly be an advantage in three dimensions. The distribution in figure 9 corresponds with figure 12 in reference 13, but the subvortex system for the present case was doubled. The higher-order geometry routine for positioning the subvortices was used, but the subvortex strength variation was linear. The calculated pressures are in good agreement with the exact solution except near the leading edge. A higher-order strength variation for the subvortices, as discussed above, should improve the calculations in the peak suction region.

Submerged Depth

The submerged depth has a significant effect on the solution. Typical variations in the errors in integrated C_L, C_M and C_D with submerged depth factor, SDF, are presented in figure 10. The errors in C_D and C_M decrease rapidly as the dpeth decreases, but the computing time increases because the

number of subvortices must increase; e.g., the time for SDF = 0.05 is 35% higher than that for SDF = 0.1. A submerged depth of about 0.1 seems a reasonable compromise.

Near-field Radius

The near-field radius factor, NRF, when multiplied by the Δ value of a basic vortex, defines a circle centered on that vortex. Whenever a velocity calculation point comes inside the circle, then that basic vortex is modified by the subvortex technique. Figure 11 shows the effect of NRF on the force and moment errors from the pressure integration. They show excellent convergence characteristics as NRF increases, although C_L appears to be converging towards an error of the order of 0.5%. The error in C_L based on circulation, however, converges towards zero. The calculated pressure distribution at the arbitrary points improves as NRF increases, but there is little visual change in the distributions from that shown in figure 7 (NRF = 5) for NRF values above about 3. Computing time decreases rapidly as NRF is reduced; a value of 3 instead of 5 for NRF gives a time saving of 30%.

CONCLUDING REMARKS

Discretization of a vortex sheet introduces significant velocity errors only within a distance from the sheet equal to the vortex spacing in the lattice. Core models applied to the vortices help to limit the size of errors but do not reduce them to a satisfactory level when the field of interest approaches close to the vortex sheet. The region where significant errors occur can be reduced to a small region of controllable width close to the vortex sheet by the use of the near-field model in which a discrete vortex splits into an increasing number of subvortices as it is approached. The combination of the subvortex technique with a concept that places the singularities inside the airfoil has resulted in a method by which accurate pressures (and velocities) can be calculated directly (i.e., without interpolation) at any arbitrary point on the airfoil surface. The method is essentially a numerical integration procedure, but, by developing it from the vortex-lattice model, a useful set of rules and automatic procedures has resulted, which makes the method accurate as well as efficient when moving from near to far-field regions. The calculations were enhanced by combining sources with the vortices.

The results obtained so far indicate that the number of basic singularities used to represent an airfoil should be of the order of 40 to 50. However, the results also suggest that the use of a higher-order strength variation for the subvortices in regions of high pressure gradient might allow the number to be decreased -- possibly as low as 20. Bearing in mind accuracy and computing effort, the optimum values for the submerged depth and for the near-field radius would appear to be of the order of 0.1Δ and 3Δ, respectively. The method could be extended to the three-dimensional case for application to vortex-lattice methods, and should then allow close-approach situations associated with multiple components and force-free wake calculations.

REFERENCES

1. Rubbert, P.E.: Theoretical Characteristics of Arbitrary Wings by a Non-Planar Vortex Lattice Method. D6-9244, The Boeing Co., 1964.

2. Maskew, B.: Calculation of the Three-Dimensional Potential Flow Around Lifting Non-Planar Wings and Wing-Bodies Using a Surface Distribution of Quadrilateral Vortex Rings. TT7009, Loughborough Univ. of Technology, England, Sept. 1970.

3. Maskew, B.: Numerical Lifting Surface Methods for Calculating the Potential Flow about Wings and Wing-Bodies of Arbitrary Geometry. Ph.D. Thesis, Loughborough Univ. of Technology, England, Oct. 1972.

4. Belotserkovskii, S.M.: Calculation of the Flow Around Wings of Arbitrary Planform over a Wide Range of Angles of Attack. NASA TTF-12, 291, May 1971.

5. Butter, D.J.; and Hancock, G.J.: A Numerical Method for Calculating the Trailing Vortex System Behind a Swept Wing at Low Speed. The Aeronautical Journal, Vol. 75, No. 728, Aug. 1971, pp. 564-568.

6. Hackett, J.E.; and Evans, M.R.: Vortex Wakes Behind High-Lift Wings. J. Aircraft, Vol. 8, No. 5, May 1971, pp. 334-340.

7. Labrujere, Th.E.: A Numerical Method for the Determination of the Vortex Sheet Location Behind a Wing in Incompressible Flow. TR 72091 U, National Aerospace Laboratory (NLR), Amsterdam, the Netherlands, July 1972.

8. Lind, I.A.: A Non-Linear Vortex Lattice Method Applicable to Three-Dimensional Wing Systems with Rolled Up Vortex Wakes in Low Subsonic Flow. FI43, The Royal Institute of Tech., Stockholm, Sweden, 1973.

9. Rehbach, C.: Calculation of Flows around Zero Thickness Wings with Evolutive Vortex Sheets. NASA TTF-15, 183, 1973.

10. Mook, D.T.; and Maddox, S.A.: Extension of a Vortex Lattice Method to Include the Effects of Leading-Edge Separation. J. Aircraft, Vol. 11, No. 2, Feb. 1974, pp. 127-128.

11. Summa, J.M.: Potential Flow about Three-Dimensional Streamlined Lifting Configurations, with Application to Wings and Rotors. SUDAAR No. 485, Stanford University, California, Sept. 1974.

12. Maskew, B.: A Subvortex Technique for the Close Approach to a Discretized Vortex Sheet. NASA TM X-62, 487, Sept. 1975.

13. Maskew, B.: A Submerged Singularity Method for Calculating Potential Flow Velocities at Arbitrary Near-Field Points. NASA TM X-73, 115, March 1976.

14. Chorin, A.J.; and Bernard, P.S.: Discretization of a Vortex Sheet with an Example of Roll-up. FM-72-5, College of Engineering, Univ. of California, Berkeley, Calif., Nov. 1972.

15. Kuwahara, K.; and Takami, H.: Numerical Study of Two-Dimensional Vortex Motion by a System of Point Vortices. J. of the Physical Soc., Japan, Vol. 34, No. 1, Jan. 1973, pp. 247-253.

16. Lan, C.E.: A Quasi-Vortex Lattice Method in Thin Wing Theory. J. Aircraft, Vol. 11, No. 9, Sept. 1974, pp. 518-527.

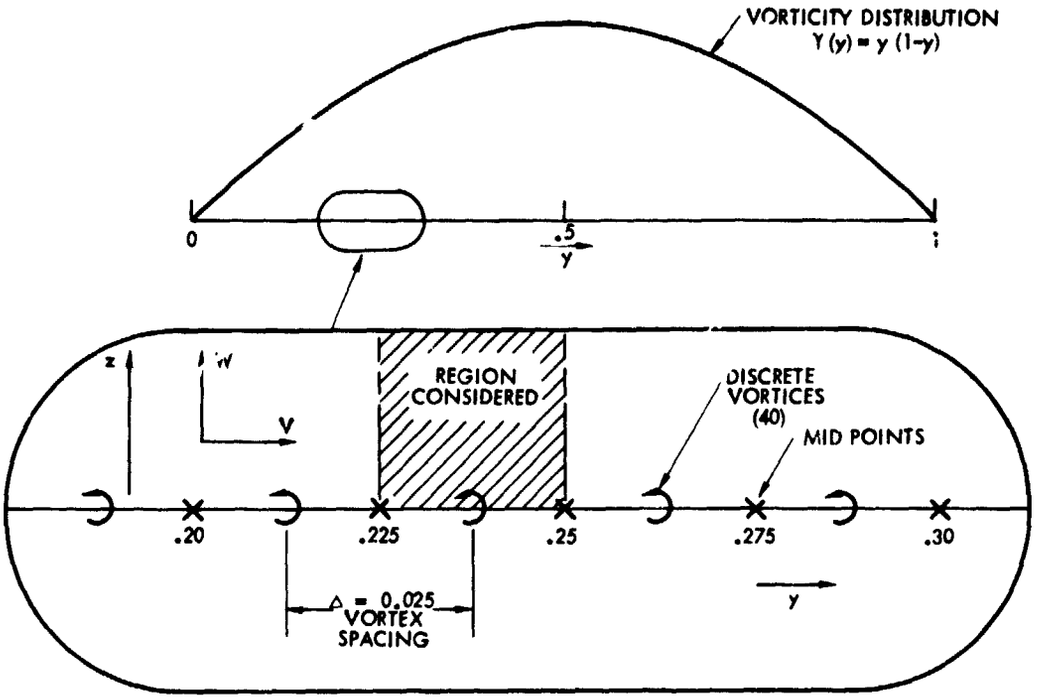

(a) Location of region considered.

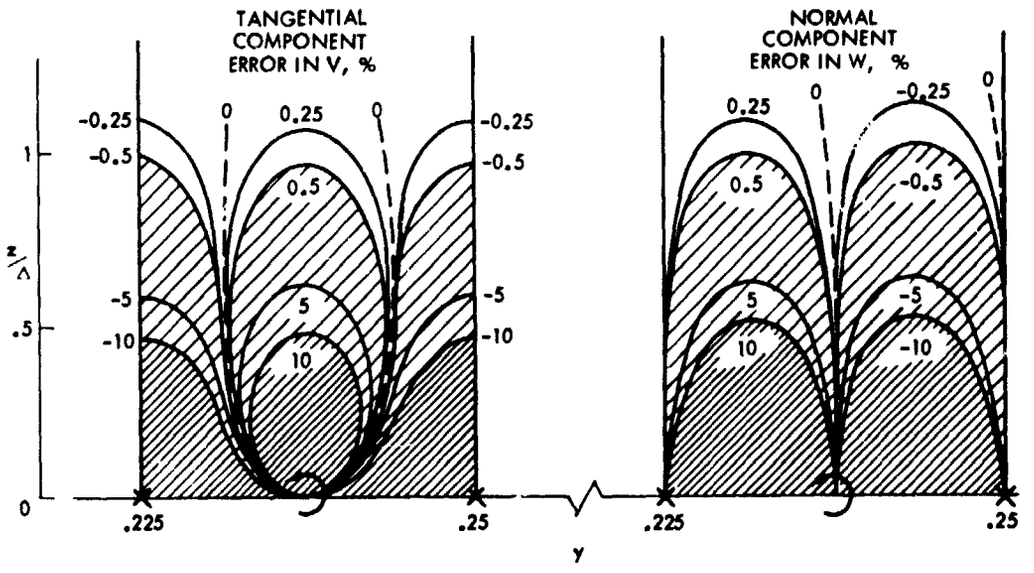

(b) Velocity error contours for the basic discretization.

Figure 1.- Velocity error calculations.

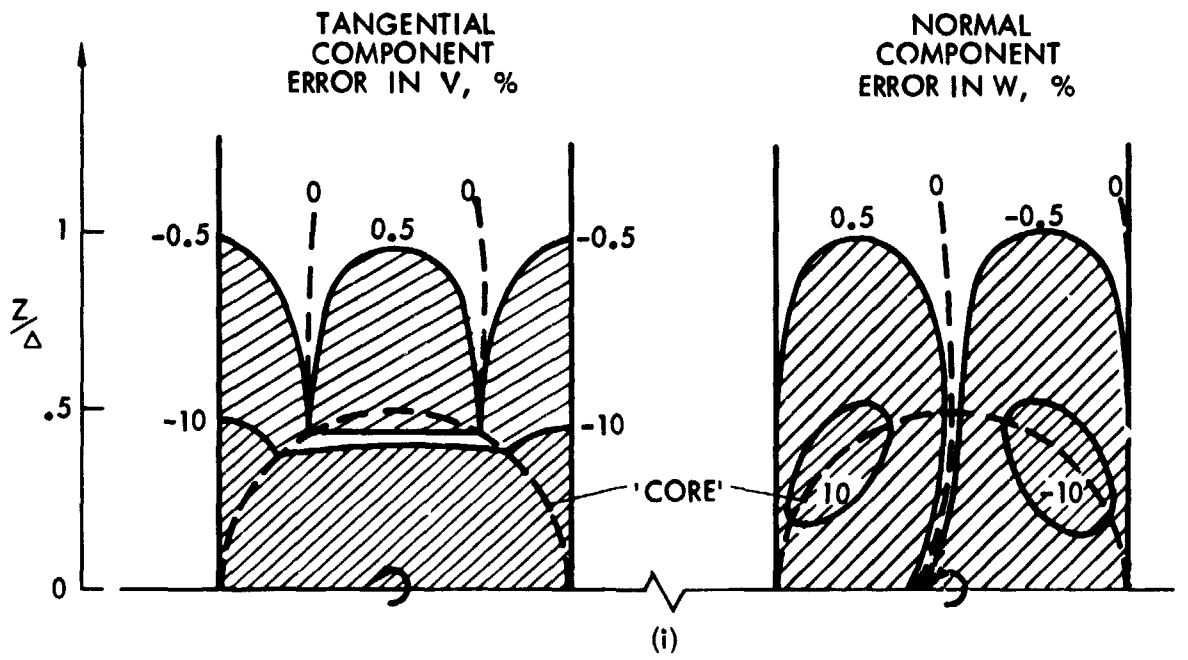

Figure 2.- Velocity error contours for a Rankine vortex core model. Core diameter = Δ.

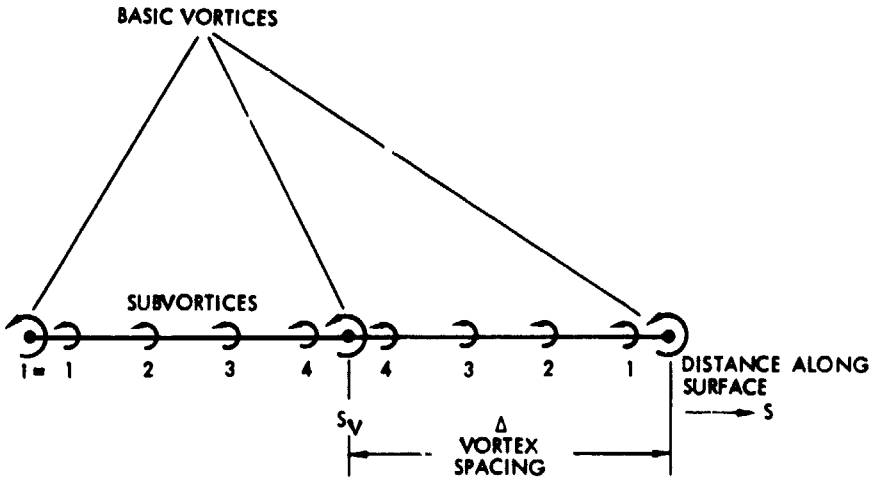

SUBVORTEX POSITIONS, $S_i = S_V \pm |NSV + 0.5 - i| \Delta / NSV$

(a) Arrangement of the subvortices for NSV = 4.

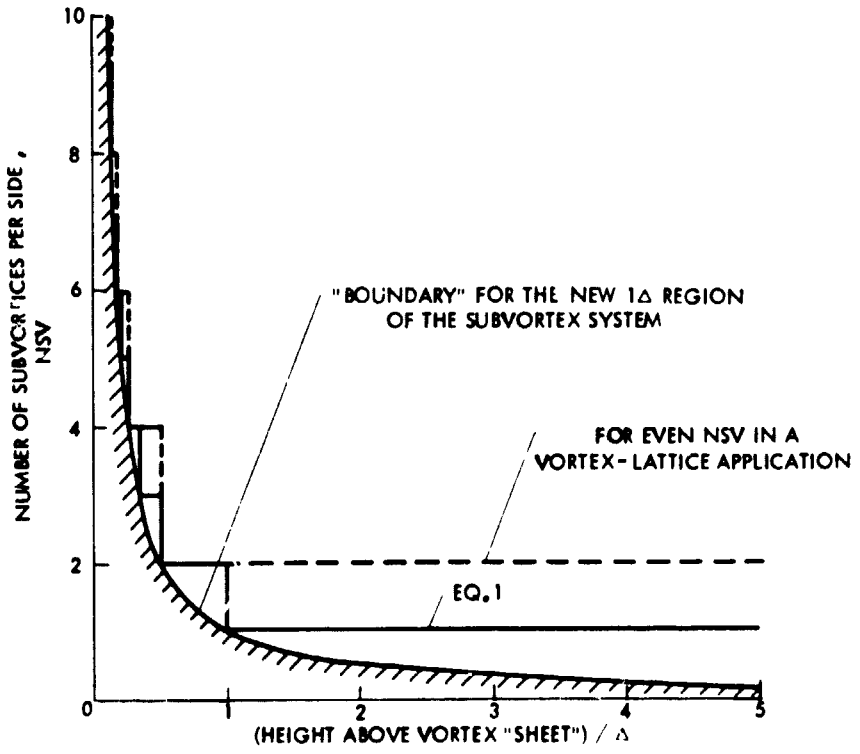

(b) Number of subvortices as a function of height above the segment.

Figure 3.- The subvortex technique.

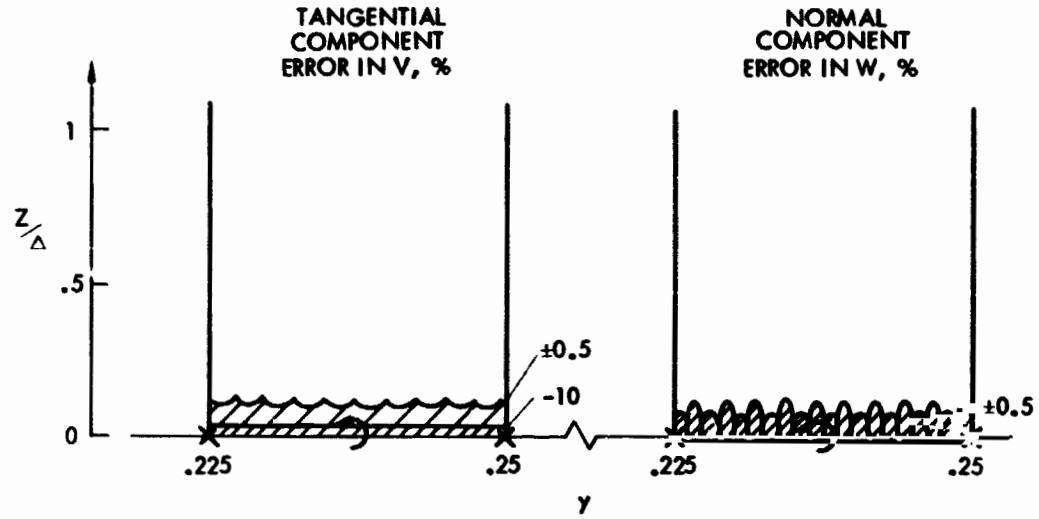

Figure 4.- Velocity error contours for the subvortex technique. Near-field radius = 5Δ. NSV_{MAX} = 10.

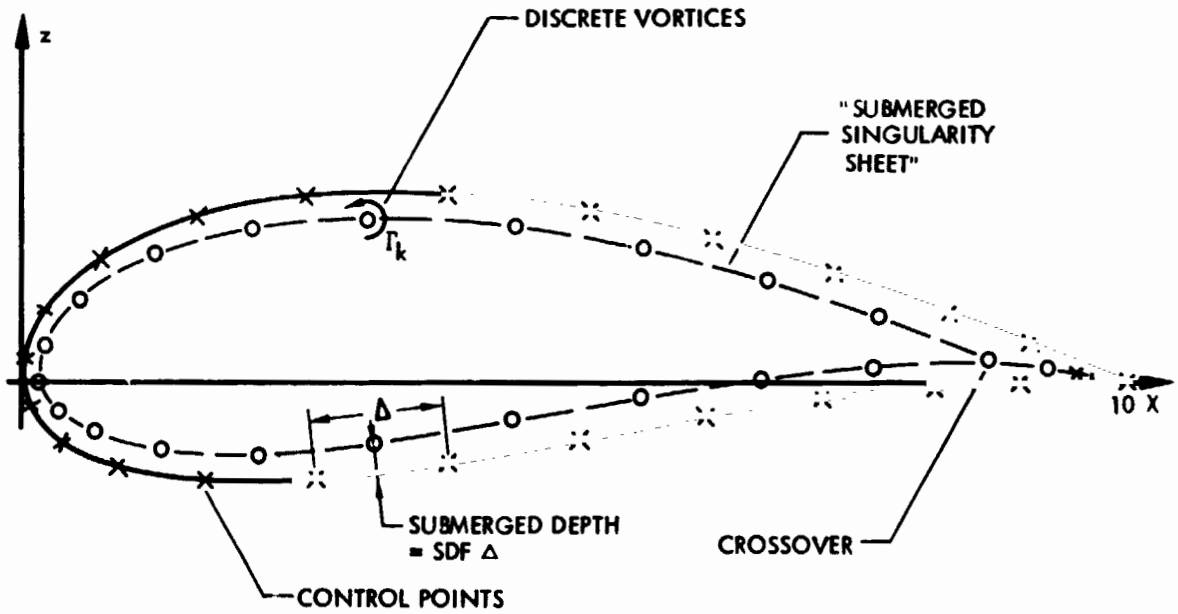

Figure 5.- Submerged singularity model with discrete vortices.

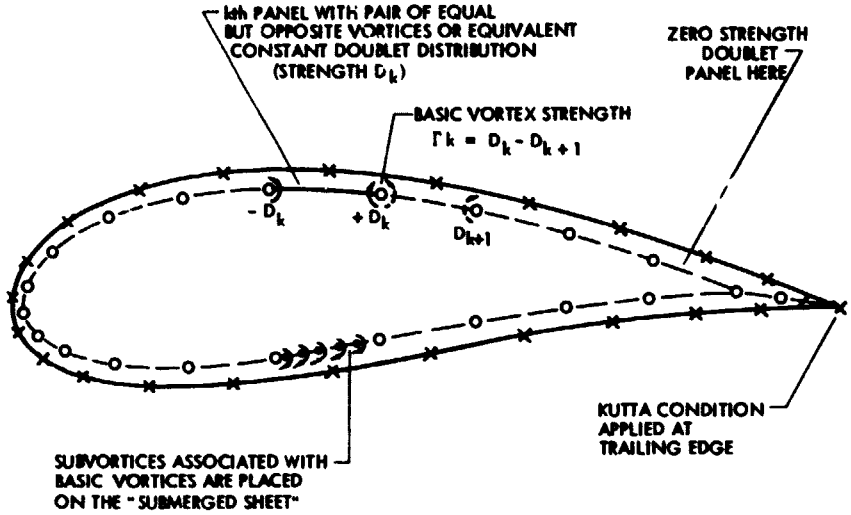

Figure 6.- Equivalent piecewise constant doublet model.

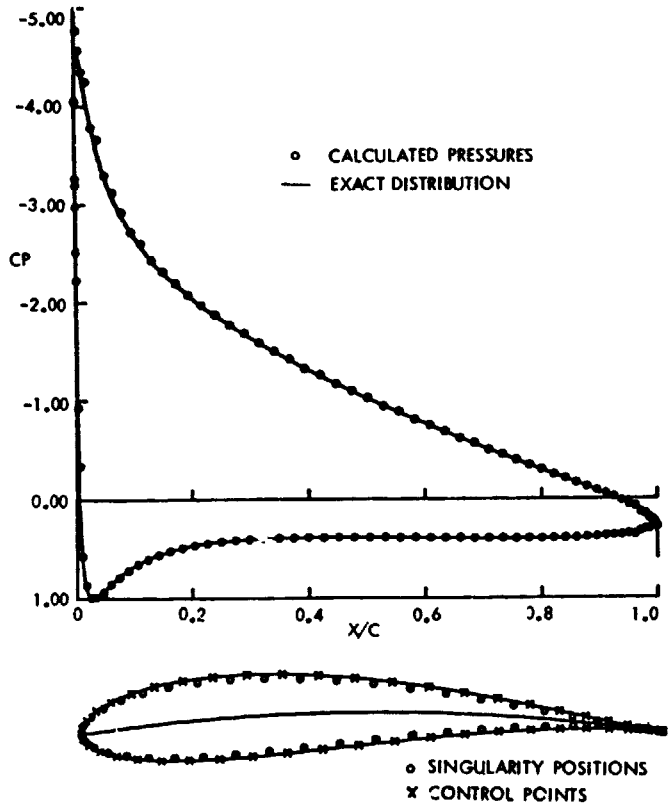

Figure 7.- Pressures calculated at arbitrary points on a Joukowski airfoil at 10^{o} incidence. Model: submerged vortices and sources (coincident) with subvortex technique applied (linear interpolation for position); 46 basic singularities; submerged depth = 0.1Δ; near-field radius = 5Δ.

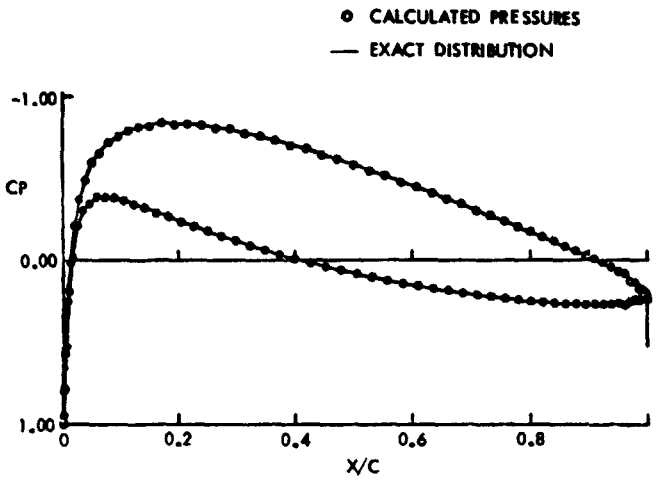

Figure 8.- Pressures calculated at arbitrary points on a Joukowski airfoil at zero incidence. Model: as in figure 7 but with higher-order interpolation for subvortex positions.

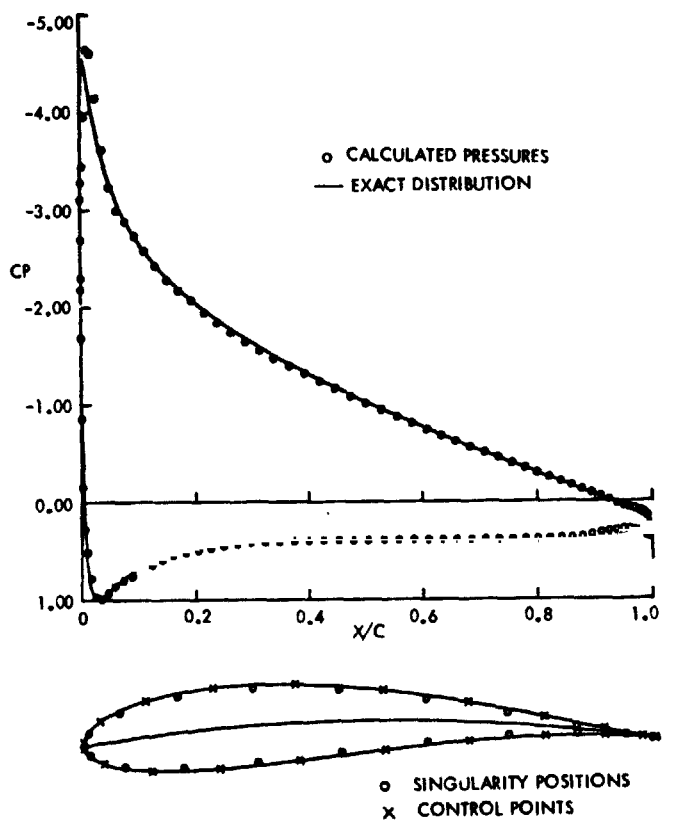

Figure 9.- Pressures calculated at arbitrary points on a Joukowski airfoil at 10^{o}. Model: as in figure 7 but with 19 basic singularities.

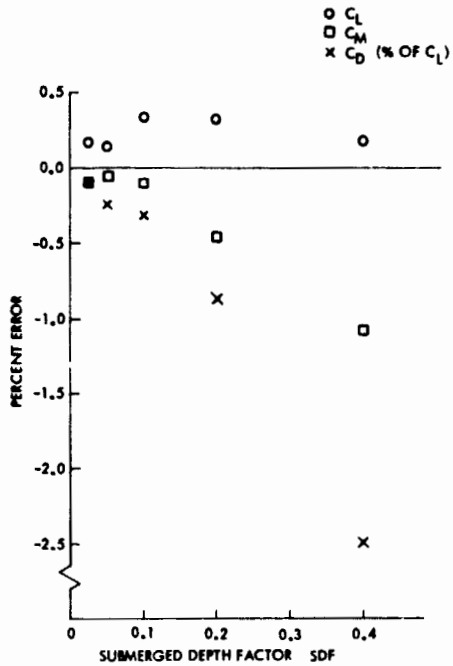

Figure 10.- Effect of submerged depth factor, SDF, on the errors in the integrated force and moment coefficients. Basic case as in figure 7.

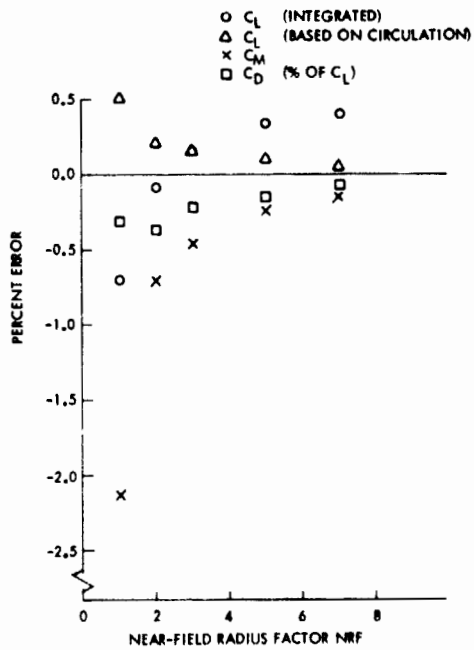

Figure 11.- Effect of near-field radius factor, NRF, on the errors in the integrated force and moment coefficients. Basic case as in figure 7.